The Descent Imager/Spectral Radiometer (DISR) Aboard Huygens

M. G. Tomasko,[1] L. R. Doose,[1] P. H. Smith,[1] R. A. West,[2] L. A. Soderblom,[3] M. Combes,[4] B. Bézard,[4] A. Coustenis,[4] C. deBergh,[4] E. Lellouch,[4] J. Rosenqvist,[4] O. Saint-Pé,[4] B. Schmitt,[5] H. U. Keller,[6] N. Thomas[6] & F. Gliem[7]

[1]*Lunar and Planetary Laboratory, University of Arizona, Tucson, AZ 85721, USA*
E-mail: mtomasko@lpl.arizona.edu Fax: +1 520 621-2994
[2]*Jet Propulsion Laboratory, 4800 Oak Grove Drive, Pasadena, CA 91109, USA*
[3]*US Geological Survey, 2255 North Gemini Drive, Flagstaff, AZ 86001, USA*
[4]*Département de Recherche Spatiale (DESPA), Observatoire de Paris, F-92195 Meudon, France*
[5]*Laboratoire de Glaciologie et Géophysique de l'Environnement, Grenoble, France*
[6]*Max Planck Institut für Aeronomie, PO Box 20, D-37189 Katlenburg-Lindau, Germany*
[7]*Technische Universität Braunschweig, D-38023 Braunschweig, Germany*

Huygens' payload includes the Descent Imager/Spectral Radiometer (DISR). In this paper, we describe the design and operation of this optical instrument, including its major science objectives and the data expected from its descent into Titan's atmosphere.

1. Introduction

Sunlight plays a key role in driving many important physical processes in planetary physics. Absorption of UV light drives photochemical reactions, leading to changes in atmospheric composition and the production of atmospheric aerosols. The size, shape, composition and distribution of aerosols and cloud particles determine their optical properties and their ability to absorb sunlight and emit thermal infrared radiation. Thus they play a key role in the atmosphere's thermal balance. The net radiative heating or cooling rate provides the forcing for atmospheric dynamics, which in turn can affect the distribution of aerosol and cloud particles and influence climate. The composition, thermal balance, dynamics and meteorology of the atmosphere also affect (and are affected by) the nature of the surface. Surface images in reflected sunlight, together with near-IR reflection spectra, can reveal the nature of the surface and its interactions with atmospheric processes. Optical measurements of solar radiation made inside a planetary atmosphere can thus reveal a great deal about many important physical processes occurring there.

The Descent Imager/Spectral Radiometer (DISR) is the optical instrument aboard Huygens that makes measurements at solar wavelengths. It was developed in a collaborative effort by scientists from the US, France and Germany. DISR measures solar radiation using silicon photodiodes, a 2D silicon Charge Coupled Device (CCD) detector and two InGaAs near-IR linear array detectors. Fibre optics connect the detectors to many separate sets of foreoptics that collect light from different directions and in different spectral regions. In this way, the instrument can collect a suite of measurements that are carefully selected to answer key questions concerning the nature of Titan's surface and the composition, meteorology, thermal balance and clouds and aerosols in Titan's atmosphere.

The purpose of this paper is to describe DISR and the scientific investigation planned for its descent through Titan's atmosphere aboard Huygens. The scientific objectives are outlined briefly in section 2 to set the context for the description of the instrumental approach contained in section 3. Section 4 summarises the measurements planned during the mission. A final section emphasises some of the connections between the measured quantities and the scientific objectives, and summarises the results expected from the investigation.

2. Scientific Objectives

2.1 Thermal balance and dynamics

A basic objective of the DISR investigation is the direct measurement of the solar heating rate's vertical profile. This will be done using measurements of the upward and downward solar flux at 0.35-1.7 μm from 160 km to the surface at a vertical resolution of approximately 2 km. The downward flux minus the upward flux gives the net flux, and the difference in the net flux at two altitudes gives the amount of solar energy absorbed by the intervening atmospheric layer. Knowledge of the solar heating profile is necessary for understanding the atmosphere's thermal balance.

Combining the solar heating profile with the thermal cooling profile provides the net radiative drive for atmospheric dynamics. The radiative cooling profile will be modelled using the temperature profile and the opacity of atmospheric gases and cloud and aerosol particles at wavelengths in the thermal-IR. The gaseous composition and temperature profile will be measured by other Huygens and Cassini instruments. The DISR measurements make an important contribution by determining the size, shape, optical properties and vertical distribution of aerosol and cloud particles. Once the solar heating and thermal cooling have been combined, model computations can be used to estimate the wind field from the radiative forcing.

Finally, DISR will measure the horizontal wind direction and speed as functions of altitude from images of the surface obtained every few kilometres in altitude, which will directly show the Probe's drift over Titan's surface. The measured wind speed and direction determined by DISR can be compared to the wind field computed from the net radiative forcing determined above.

2.2 Distribution and properties of aerosol and cloud particles

Several properties of the cloud and aerosol particles are important for understanding their interaction with the solar and thermal radiation field. The particle sizes compared to the radiation's wavelength is important for understanding particle scattering. Measurements of both the forward-scattering and polarising nature of Titan's aerosols have been used to show that spherical particles cannot simultaneously explain these two types of observations (see Hunten et al., 1984; West & Smith, 1991). Information on particle shape in addition to size is therefore required for understanding particle scattering. The vertical distribution of the particles also influences the profiles of solar and thermal radiation. Finally, a suite of optical properties as functions of wavelength is needed to permit accurate computations of the particles' interactions with radiation. These properties include the optical depth, single scattering albedo and the shape of the scattering phase function. The variation of these optical properties with wavelength, together with determinations of size and shape, can yield the imaginary refractive index and thus constrain the composition of the particles.

DISR will measure many of these properties using combinations of measurements of small-angle scattering in the solar aureole in two colours, measurements of side- and back-scattering in two colours and two polarisations, measurements of extinction as a function of wavelength from the blue to the near-IR, and measurements of the diffuse transmission and reflection properties of layers in the atmosphere as outlined in sections 3 and 4.

2.3 Nature of the surface

Titan's surface was hidden from the Pioneer and Voyager cameras by the layers of small haze particles suspended in the atmosphere. Nevertheless, intriguing suggestions regarding the nature of the surface have been made (Lunine, 1993), including the possibility that it consists of a global ocean of liquid methane-ethane. Recent radar observations (Muhlman, 1990) and direct observations at longer wavelengths (Smith et al., 1996; Lemmon et al., 1995) strongly hint that the surface is not a global ocean. The many fascinating surfaces observed by Voyager on satellites of the outer solar system showed a surprising range of phenomena, including craters, glacial flows, frost and ice coverings, and active geysers and volcanoes. This preliminary exploration of the small bodies of the outer solar system suggests that Titan's surface may well also contain surprises.

DISR will determine the surface's physical state (solid or liquid) near the impact site, and determine its fraction in each state. DISR will measure the topography, hopefully revealing some of the physical processes that have formed the surface. DISR will obtain reflection spectra of surface features from the blue to the near-IR in order to constrain the composition of the different types of terrain observed. In addition, DISR will image the surface at resolution scales from hundreds of metres (similar to those from the Orbiter) to tens of centimetres over as large an area as possible to permit studies of surface physical phenomena and to clarify surface-atmosphere physical interactions.

2.4 Composition of the atmosphere

Huygens carries a Gas Chromatograph Mass Spectrometer (GCMS) for direct measurement of the atmosphere's composition. Nevertheless, direct sampling techniques can give inaccurate mixing ratios for condensable constituents if a cloud particle enters and slowly evaporates in the inlet system. DISR provides an important complementary capability for measuring the mixing ratio of methane, the most likely condensable constituent, using a technique that is not subject to this potential problem. It will be obtained from the increasing depth of methane absorption bands as the gas path between the instrument and top of the atmosphere increases during descent.

Methane can exist as a solid, liquid or gas on Titan, and has been suggested as playing a role in Titan's meteorology similar to the role played by water on Earth. DISR's measurements of the methane mixing profile will be analogous to a relative humidity profile on Earth. Finally, Titan's atmosphere is believed to consist primarily of nitrogen, methane and argon. DISR's measurements of methane's mixing ratio, together with determination of the atmosphere's total mean molecular weight by radio occultation measurements made by the Cassini Orbiter, will indirectly yield the argon to nitrogen mixing ratio as an important backup to Huygens' mass spectrometer measurements.

3. Instrument Approach

3.1 General

In order to achieve this broad range of scientific objectives, it is necessary to measure the brightness of sunlight in Titan's atmosphere with several different spatial fields of view, in several directions and with various spectral resolutions. For measurements of solar energy deposition, for example, measurements are needed of the downward and upward solar flux with broad and flat spectral sensitivity, and with a cosine zenith angle weighting. For determination of the surface's composition, spectral resolution is desirable and spatial information is necessary. For determination of the physical processes occurring on the surface, images are needed with very broad fields of view looking down toward the surface. To determine the size distribution of aerosol particles above the Probe's altitude, upward measurements are needed of the brightness of the

sky near the Sun (the solar aureole) in at least two colours with modest angular resolution. Images looking out towards the horizon are useful for sensing the presence of thin haze layers during descent.

It is not possible to include separate instruments devoted to each of these scientific objectives in Huygens' limited payload. Nevertheless, it has been possible to increase the usefulness of the single Huygens optical instrument considerably by making extensive use of fibre optics to collect light from different directions and bring it to a few centrally-located detectors after various spectral or spatial analyses. In this way, redundant electrical systems have been minimised and moving mechanical parts have been all but eliminated. A summary of the locations of the fields of view and spectral coverage of DISR's optical measurements is given in Table 1, while the onboard sources are summarised in Table 2.

Table 1. Summary of DISR instruments.

Upward-Looking Instrument	*Azimuth Range*	*Zenith Range*	*Spectral Range (nm)*	*Spectral Scale (/pixel)*	*Spatial Scale (/pixel)*	*Pixel Format*
Violet Photometer (ULV)	170°	5-88°	350-480	—	—	1
Visible Spectrometer (ULVS)	170°	5-88°	480-960	2.4 nm	—	8×200
Infrared Spectrometer (ULIS)	170°	5-88°	870-1700	6.3 nm	—	132
Solar Aureole (SA 1) Vertical Polarisation	6°	25-75°	500±25	—	1°	6×50
Solar Aureole (SA 2) Horizontal Polarisation	6°	25-75°	500±25	—	1°	6×50
Solar Aureole (SA 3) Vertical Polarisation	6°	25-75°	935±35	—	1°	6×50
Solar Aureole (SA 4) Horizontal Polarisation	6°	25-75°	935±35	—	1°	6×50
Sun Sensor (SS) (64° cone FOV)	64° cone	25-75°	939±6	—	—	1
Downward-Looking Instrument	*Azimuth Range*	*Nadir Range*	*Spectral Range (nm)*	*Spectral Scale (/pixel)*	*Spatial Scale (/pixel)*	*Pixel Format*
Violet Photometer (DLV)	170°	5-88°	350-480	—	—	1
Visible Spectrometer (DLVS)	4°	10-50°	480-960	2.4 nm	2°	20×200
Infrared Spectrometer (DLIS)	3°	15.5-24.5°	870-1700	6.3 nm	—	132
High-Resolution Imager (HRI)	9.6°	6.5-21.5°	660-1000	—	0.06°	160×256
Medium-Resolution Imager (MRI)	21.1°	15.75-46.2 5°	660-1000	—	0.12°	176×256
Side-Looking Imager (SLI)	25.6°	45.2-96°	660-1000	—	0.20°	128×256

Table 2. Summary of DISR onboard sources.

System	*Number of Lamps*	*Power each*	*Field*	*Spectral Range (nm)*	*Optics*
Inflight Calibration	3	1 W	Fills each instrument FOV	400-2000	f/2 fibre feed
Surface Science Lamp (SSL)	1	20 W	4×12° centred on DLIS FOV	400-2000	50mm parabola
Sun Sensor Stimulator	1	10 mW diode	Illuminates only Sun Sensor detector	939±6	feeds fibre

One of the detectors around which DISR is built is a 512 × 520-pixel CCD silicon detector with a 400-1000 nm wavelength response. The CCD's surface is divided into nine separate regions, with the light collected by different foreoptics and brought to the detector by fibre optic bundles and ribbons. These include imagers looking in three different directions with different fields of view and angular resolutions, two regions fed by light collected by upward- and downward-looking grating spectrometers for flux measurements and for making spatially-resolved spectra of the surface at 480-960 nm, and four regions devoted to measurements across the solar aureole in two colours and in two different polarisation states.

The second type of DISR detector is a pair of 150-element InGaAs near-IR linear arrays. They are mounted side by side in the focal plane of a second grating spectrometer covering 870-1650 nm. This spectrometer is also fed by two sets of optical fibres collecting:

1. the downward flux from a horizontal diffusing flux plate sensitive to half the upper hemisphere
2. the brightness of a strip on the ground defined by the input slit, which provides a measure of the upward flux as well as the reflectivity of a well-defined ground region.

The third detector type comprises single silicon photodiodes with enhanced UV response to extend the upward and downward flux measurements to 350 nm from the short wavelength limit of the visible spectrometer at 480 nm. This type of detector is also used in a separate optical system to detect the Sun's azimuth for controlling data collection timing.

We begin a more detailed discussion of the instrument by turning first to the detectors around which DISR is built. Other significant aspects of the instrument are reviewed in turn.

3.2 CCD detector

Co-Investigator Dr H. U. Keller of the Max Planck Institut für Aeronomie (MPAE) in Germany is responsible for the CCD subsystem, including the CCD itself and the electronics to clock and read out the detector. MPAE contracted with Loral Fairchild to supply the flight CCDs. The data interface between the German and US electronics is at the output of the 12-bit analogue-to-digital (A/D) converter.

The format of the frame transfer CCD is shown in Fig. 1. The CCD is a modification of a standard 512 × 512-pixel two-phase scientific imager. Seven masked columns and one grey (transition) column are added on the right side of the detector face. It is divided into an image section and a memory, or storage, section, each 256 × 520-pixels in size. The image section requires anti-blooming drains to provide protection from the excess charge produced when the Sun flashes through the solar aureole section. The anti-blooming drain takes up 6 μm on the side of each pixel. The individual pixels are 17 × 23 μm (sensitive area) on 23 μm centres. The CCD input is via a coherent fibre optic bundle with 6 μm core size and 8 μm centre-to-centre spacing. The CCD is fed by optical fibres from nine optical subsystems: HRI, MRI, SLI, ULVS, DLVS and the 4-channel SA radiometer (two colours in each of two orthogonal polarisation states). The detector has a relative spectral response typical for silicon, and is sensitive between 400 nm and about 1000 nm, depending on temperature. The quantum efficiency of the CCD material is also typical for silicon and quite good ($\sim$50%) at peak.

Exposure time is controlled solely by rapid (0.5 ms) shifts of the charge from the top half to the bottom half of the chip, which is covered by an opaque metal film. The exposure time (typically between 10 ms for images and 500 ms for spectra) is the time between rapid shifts. No mechanical shutter is needed and no moving parts are used

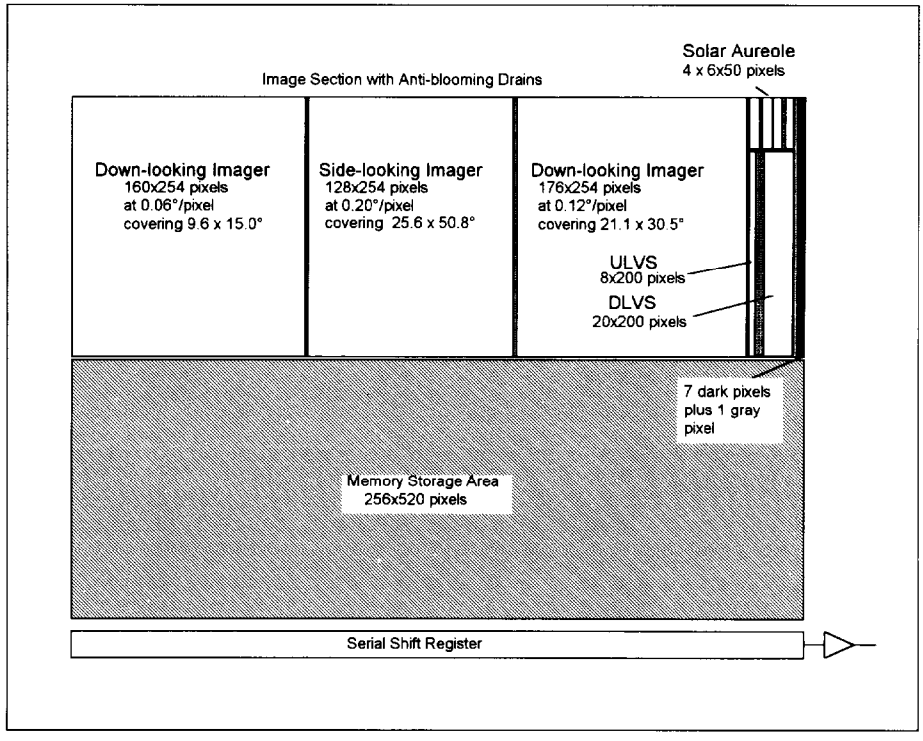

Fig. 1. Layout of the CCD detector face.

in this system, a feature that makes possible the use of different foreoptics for many different functions all using the same CCD. The full CCD frame is read out and digitised for imaging data, a process that takes about 2.2 s for the entire frame. Only the first 49 columns are digitised for taking spectra and solar aureole measurements, thus shortening the readout time to about 300 ms when only these measurements are made.

The CCD pixel signals are pre-amplified in the Sensor Head (SH) to minimise the possibility of noise. After amplification, the signals are relayed over a short connecting cable to the Electronics Assembly (EA), where they undergo video processing, including correlated double sampling. A fast 12-bit A/D converter digitises the pixels, which are clocked to the bus. After A/D conversion, a pseudo-square root algorithm reduces the imaging data from 12 to 8 bits/pixel. The image data are then compressed in a lossy hardware compressor. The compression factor is programmable, and will be between 3:1 and 8:1 for different images. The spectral and solar aureole data from the CCD are compressed with a lossless software compression algorithm from 12 to about 6 bits/pixel depending on the entropy of the data, and then buffered for transmission.

The dark current from the CCD is measured by the signals from the column of masked pixels along the chip's edge. These data are read out and transmitted to the ground once every data cycle (about every 1½-3 min). At Titan entry, the chip is at a temperature of some 260K, and the dark current is a few per cent of typical signals. After some 40 min, the detector cools to <200K, and the dark current is essentially negligible.

The full well capacity of the CCD pixels is about 125 000 electrons. This is digitised to 12 bits for 4096 levels of some 30 electrons/step (before square root compression). The read noise of the system (CCD, electronic amplifiers, sample and hold, A/D conversion and subsequent handling) is <23 electrons. The data are shot-noise limited for all but the lowest signals.

3.3 IR detector

The focal plane assembly consists of two linear photodiode arrays (one dedicated to DLIS and the other to ULIS) along with their associated pre-amplifier electronics. Each array contains 150 individual InGaAs photodiodes connected to CCD readout registers. The detector arrays include thin titanium masks to protect the CCD multiplexers from visible stray light. Each detector chip is bonded onto a sapphire substrate. The two elementary modules, consisting of the detectors plus CCD on the sapphire base, are assembled on a ceramic base and protected by a hermetically sealed titanium case that includes a coated glass window. A copper thermal lug bonded at the rear of the ceramic base and connected by a thermal strap to Huygens' exterior is used for cooling the detector assembly. A silicon diode bonded onto the ceramic base provides a measure of the focal plane array's temperature. The detector assembly is mounted on a printed wiring board connected through a flex cable to the IR pre-amplifier board in the Sensor Head. Each pixel has a photo-active area of 38×300 μm; the pixel pitch is 52 μm. The detector assembly was manufactured by Thomson-TCS (Saint Egreve, France). The general design is based on the technology used in the Spot 4 Earth observation satellite (Bodin & Reulet, 1987). The length of the InGaAs photodiodes has been increased by a factor of 10 relative to Spot's detectors to improve the signal-to-noise ratio (S/N) at the lower brightness level of Titan's spectrum. The IR pre-amplifier board in the Sensor Head and the clocking electronics (on a board in the DISR Electronics Assembly) were built by AETA (Fontenay-aux-roses, France).

The detector arrays are used for detecting radiation covering 850-1700 nm. Detector quantum efficiencies of around 50% were measured at 850 nm for the photodiodes; $>80\%$ were found for 1000-1500 nm. The cutoff wavelength varies linearly with temperature. The 50% level of quantum efficiency is reached at 1620 nm at 180K, and 1690 nm at 270K.

Between readouts of the photodiodes, charge is accumulated due to dark current and at a rate proportional to the flux of incident photons. The charge generated between readouts is digitised using a 14-bit A/D converter. The gain is 920 electrons per digital step with a full scale of some 14 million electrons. The dark current in the InGaAs diodes decreases roughly by a factor of 2.5 for every 10K decrease in temperature. Measurements at 270K show dark currents in the range 0.5-2 pA. The dark current is so low that even near room temperature saturation due to dark current alone requires as long as 0.1-0.4 s between reads. Somewhat larger dark currents are expected at Titan as a result of the impact of energetic protons during cruise. The minimum time between reads is 8 ms, which is sufficiently short that only a small fraction of the wells contain dark current at the 260K expected at the start of Titan descent. After some 40 min, detector temperature decreases to 200K, and dark current is almost negligible.

A shutter mechanism (the only moving part in the entire DISR) at the entrance slit of the IR spectrometer permits separate measurements of the dark signal alone and the dark plus light signal throughout the descent. Spectra with shutter open and closed are both included in the telemetry stream. The photon flux is obtained by subtracting one spectrum from the other. In addition, four pixels at the beginning and end of the array are masked with an opaque resin and provide a measure of the typical dark current, assuming that they are representative of the rest of the array. In case of shutter failure, they would provide an estimate of the dark current that can be used to remove the dark signal from shutter-open spectra obatained at warm temperatures.

The readout noise of the CCD register includes the noise associated with the various capacitances, the output amplifier and the transfer noise. It has been measured to be $\sim$1100 electrons for temperatures <270K. The shot noise is generally lower than the readout noise. About 10% of the pixels exhibit, in addition, a 1/f noise due to defects

in the p-n junction of the diode itself. Its amplitude is roughly proportional to the dark signal and amounts to 0.1-1% of the dark level.

3.4 Violet detectors

The CCD and IR array spectrometers cover 480-1700 nm. There is considerable interest in the radiation shortward of 480 nm, which is strongly absorbed by aerosols in the upper stratosphere. As there are only extremely weak methane bands in this part of the spectrum, high spectral resolution is not required. Two silicon photodiodes, appropriately filtered so that the 350-480 nm bandpass gives a flat spectral response, measure the flux in the upward- and downward-viewing directions. The ULV detector is behind the input diffuser of the ULVS. The DLV detector requires a separate window from the DLVS, with a diffuser plate and baffle system to define its π steradian field of view (FOV).

3.5 DISR sub-instruments

3.5.1 Imagers

The design of the imagers is driven by several considerations. The range to Titan's surface decreases by three orders of magnitude during the descent from 160 km at entry to only a few hundred metres at the last image. Even the 160 km maximum range is orders of magnitude less than is typical for images of planetary surfaces obtained by any other technique, including close flybys. Thus, the usual requirement for high angular resolution, necessary for observations made at longer range, are much relaxed in our case. We have chosen a maximum angular resolution of 0.06°/pixel, similar to that of the naked human eye. This pixel size of about 1 mrad gives a spatial scale of 160 m/pixel at descent start and about 20 cm/pixel at 200 m. The low resolution overlaps that available from orbiters and the high resolution near impact is three orders of magnitude greater.

Given the limitation of only 256 pixels across the CCD's active area, even this relatively low angular resolution would limit the coverage in a single image to 15°. In order to observe as large a surface area as possible, we have chosen to divide the CCD's long dimension into three image frames centred at different angles from the nadir that, together, cover the range of nadir angles from 6.5° to 96°. This is done with the division shown in Table 1. As the Probe rotates, sets of three images can be obtained at 12 azimuths to give a panorama with full coverage over nadir angles from 6.5° to 75°. A set of 24 images in azimuth, obtained in two staggered sets of 12 in successive measurement sets, permits full coverage in azimuth for the most side-looking imager and also completes the mosaic from nadir angles of 6.5° to 96°. The footprints of the individual images in a panoramic mosaic are shown in Fig. 2.

The size of the imager pixels and their nadir angles define the relationship between integration time and blurring due to Probe rotation during image exposure. We limit the integration time so that rotation during exposure is $\sim$1.5 times the angular size of a pixel in the centre of the High-Resolution Imager's FOV. The blur in the other imagers is $\leq$ that in the HRI.

This limitation on integration time translates into a relation between the f/number of the optical system and the S/N ratio in the images for a model of the brightness of Titan's surface. We selected an f/2.5 system to permit S/N $\geq$ 100 at the rotation rate of 1.5 rpm expected at low altitudes for a nominal model of Titan's surface and the quantum efficiency and transmission expected for the imaging system.

For good imaging, we require that the optical systems be capable of giving spot sizes (full width at half maximum) smaller than two CCD pixels. The spot size is produced by geometrical aberrations in the lenses, diffraction and the spreading of light between the back face of the fibre bundle and the CCD's surface. So long as the end of the fibre

optic bundle is within 20 μm of the CCD's face, spot sizes smaller than two pixels can be achieved.

The light is brought from the three separate lens assemblies to the CCD face by a fibre optic bundle produced by Collimated Holes, Inc. The fibres are small compared to the 17×23 μm active area of the CCD pixels, so that many (about six) fibres feed each pixel. Extramural absorption is added between the clad fibres to absorb light that might emerge from individual fibres. The glass used for the fibre optic conduit is specially selected for its resistance to darkening from energetic particle impact.

The imagers' spectral range is limited to wavelengths between 660 nm and about 1000 nm. The long wavelength end is defined by the limit of the CCD detector. The short wavelength end is selected to prevent Rayleigh scattering by the atmosphere below the Probe from dominating the signal due to light reflected directly by the surface. All three imagers have the same spectral range. Colour can be added to the monochromatic images using measurements of spectral reflectivity of the surface measured by the DLVS. We plan to correlate the spectral measurements of several thousand surface points with the morphology of these points as seen in the images to produce a colour library as a function of the type of terrain (craters, canyons, lakes, stream beds, etc). In this way, surface colour images can ultimately be made from our measurements.

As described below, we expect to obtain >500 separate surface images that can be assembled into 36-image panoramic mosaics every few km from the start of descent at 160 km altitude.

3.5.2 Visible spectrometer

Measurements of the spectrum of the upward- and downward-streaming sunlight as

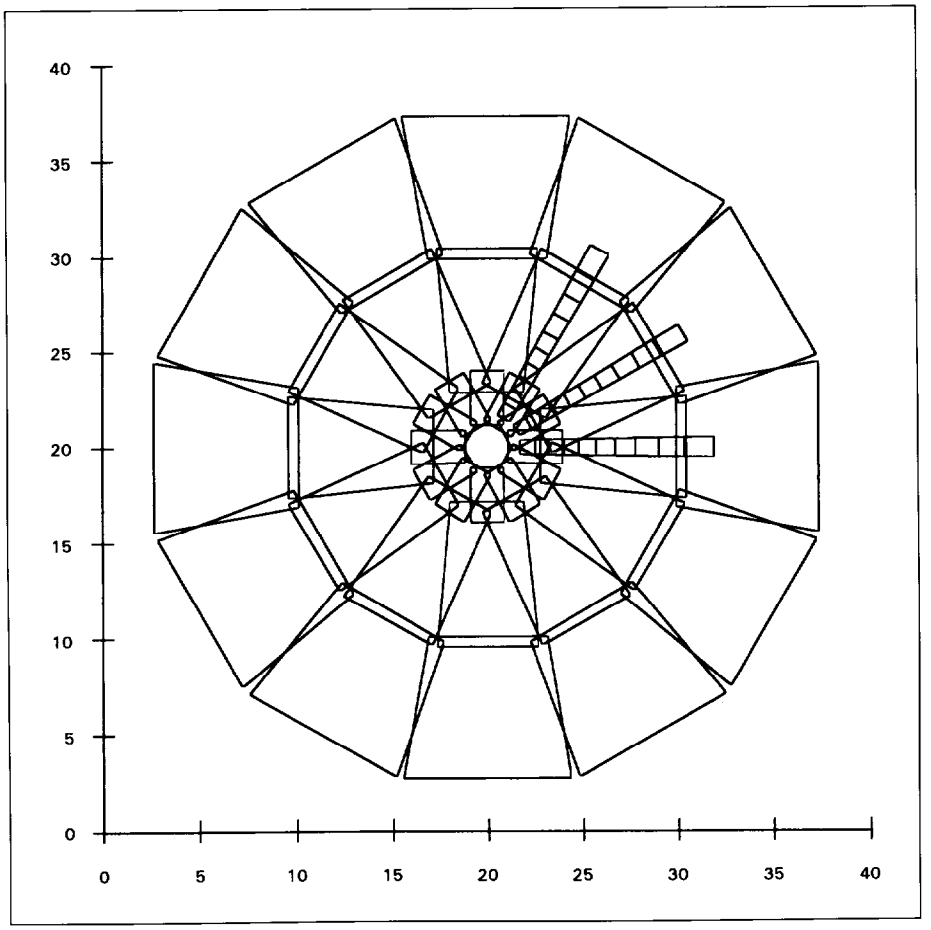

Fig. 2. Arrangement of images obtained at 12 azimuths relative to the Sun to form a panoramic mosaic. DISR also measures the surface spectral reflection at ten $4 \times 4°$ locations along the slit of the DLVS at each of the 12 azimuths. (The locations of these spectral measurements are shown at only three azimuths here for clarity.)

functions of altitude during descent support most of DISR's scientific objectives, including:

1. measurement of the solar energy absorption profile
2. measurement of methane's vertical profile
3. measurements of the optical properties, size and vertical distribution of atmospheric aerosols and clouds
4. measurements of the composition and nature of Titan's surface.

Accordingly, significant effort and experiment resources have been devoted to this portion of the instrument.

The visible spectrometer uses separate fibre bundles to bring downward- and upward-streaming sunlight to adjacent positions along the entrance slit. The speed of the collimator and camera optics of the transmission grating spectrometer is f/2. A tipped flat plate is included in the beam just before the grating to decrease the sensitivity of the measured intensity to the state of the incident light's linear polarisation. The spectral range is limited by a filter to 480-960 nm in first order. The upward- and downward-viewing spectra are focused on the ends of two fibre optic ribbons that join the fibre conduit used for the imagers. The spectra are spread over 200 CCD pixels in the spectral direction. The spectral spread function has a width (Full Width Half Maximum, FWHM) of two pixels. The resulting resolving power of the spectrometer, $\lambda/\Delta\lambda$, is 100 at the blue end and 200 at the red end of the spectrum.

The input optics used to collect the light from the upward and downward directions are quite different. In the upward-looking case, the design is driven by the desire to measure the downward-streaming flux. Thus, a horizontal diffusing plate is viewed by the input optical fibres using a small lens. The diffuser makes the angular response function similar to the ideal response function (proportional to the cosine of the zenith angle). As the instrument protrudes only slightly from the Probe, a baffle is used to limit the range of azimuth angles to 170°. This baffle is blackened to minimise skylight reflection from the baffle to the diffuser. The range of zenith angles accepted by the baffle is from 5° (to avoid seeing the parachute overhead) to 88°. Measurements made with the instrument's optical axis within 85° of the Sun direction include both the diffuse and direct solar beam. A shadow bar ($\sim$10° wide) is mounted over the diffusing plate. Measurements made with the Sun behind the shadow bar and again with it out from behind the bar permit separation of the direct and diffuse downward solar fluxes in the half of the upper hemisphere centred on the Sun. An additional measurement is also made with the instrument's optical axis directed 180° away in azimuth from the Sun to give the portion of the downward diffuse flux coming from this half of the upper hemisphere.

For the measurements in the downward direction, other considerations become important. Because we want to study the reflection spectrum of distinct regions on the ground, spatial resolution is as important as the determination of upward flux. We therefore chose to image the spectrometer's slit on the ground and to spread the light along the slit over 20 CCD pixels. Thus, we can spatially resolve 10 regions along the slit on the surface. The slit is boresighted along the vertical axis of the imagers' field to provide the morphological context of the spectrally-measured regions. The slit is 4° wide and extends from 10° to 50° nadir angle. The 40° nadir angle range covering 20 CCD pixels gives 10 resolution elements, each 4° square on the ground. The spectral intensities measured can be weighted with the cosines of the known nadir angles and integrated in nadir angle. At least eight different evenly-spaced azimuths are measured to permit an integration in azimuth for the upward flux. Thus, the optics and the sampling scheme permit integration of the spectral radiation field for the upward flux and also provide spatially-resolved measurements of the surface's spectral reflectivity.

Upward and downward spectra are obtained roughly every 2 km during the descent from 160 km altitude. In the upward direction, the integration times for the measurements under the shadow bar are limited to ensure that the measurements are completed while the diffuser is completely shaded. In the down direction, the integration times are limited so that Huygens does not rotate more than 1.5 times the angular width of the spectrometer slit at a nadir angle of 30° (the slit centre) during the integrations. The f/2 system permits S/N ≥ 100 in a single spectral and spatial pixel for the downward-looking spectrometer. For the upward-looking measurements, eight CCD detector pixels are combined along the length of the slit (which has no spatial resolution for the ULVS) to give similar S/Ns for the ULVS and DLVS.

3.5.3 IR spectrometer

The IR spectrometer has two channels: the Upward-Looking Infrared Spectrometer (ULIS) and the Downward-Looking Infrared Spectrometer (DLIS). There are two entrance paths, one viewing upward and one downward, in order to measure both the upward and downward fluxes. The ULIS has a diffuser as the entrance window (as for the ULVS), viewing about half of the upward hemisphere. This allows the measurement of flux directly, without the uncertain conversion from intensity to flux. The downward-looking input has a fused silica window and input lenses that define the FOV at the spectrometer's entrance slit. The input optics of these instruments transfer IR radiation through fibre optics to two aligned 104×300 μm entrance slits placed one after the other. The two slits of the Up and Down channels are perpendicular to the grating's dispersion plane. A shutter is installed just inside the input slits. An f/2 collimator lens assembly focuses the beams on to the transmission grating, and a camera lens assembly focuses the dispersed light on to the IR focal plane array. The IR spectrometer uses transmission gratings working in first order with achromatic lenses. A polarisation compensator, consisting of a coated tilted plate, is included in the collimated beam in front of the grating. Both the upward- and downward-looking spectra are imaged directly on the two linear arrays of InGaAs detectors through a sapphire window with anti-reflection coating.

The optical FOV of ULIS is defined by the diffuser and external baffles and is 170° in azimuth by 83° in zenith angle (from 5° to 88° zenith). The spectrometer slit of DLIS maps into a $3 \times 9°$ FOV (pixel footprint) with the FOV centre pointed 20° from the nadir.

In the case of ULVS, the exposure time is sufficiently short that an adequate exposure is possible under the narrow shadow bar even when the Probe is rotating at its maximum 15 rpm. In the case of ULIS, the total integration time is of the order of 60 s. Thus, no shadow bar is used to separate the direct and diffuse downward flux. Instead, measurements are accumulated in four azimuthal sectors relative to the Sun, and the shade provided by Huygens itself is used to separate the direct and diffuse downward flux in ULIS.

In the normal operation mode, the total time for data collection is an integral number of Probe rotations, but is always constrained to be 1-3 min. The time for data collection is estimated at the beginning of each cycle, and is updated during the cycle based on the data from the Sun Sensor after each rotation.

Within each azimuthal region, data are collected alternately with the shutter closed and with it open. The process is symmetrical in time so that linear drifts in temperature (and hence dark current) are accounted for when the shutter-closed data are subtracted from the shutter-open data. The total shutter-open time is equal to the shutter-closed time. Within each azimuth region, the process begins and ends with the shutter closed for half the time used for the other open and closed intervals. Within each shutter-open or shutter-closed interval, the IR array can be read more than once (depending on rotation period and temperature) to avoid saturation by the dark current. In addition,

the shutter rate is kept to about 5 Hz so that temperature variations beyond linear drifts and their changes in dark current are adequately compensated.

3.5.4 Solar Aureole camera

The Solar Aureole (SA) camera will measure the intensity of scattered sunlight over a range of scattering angles sensitive to particle size. Scattering at small angles ($<40°$, depending on particle size) is a good diagnostic of particle projected area. The forward-scattering lobe is more strongly peaked at small scattering angles as the particle radius increases. Its width does not depend strongly on particle shape for equal projected area particles, and it is insensitive to the particle refractive index.

Particle shape effects are much more pronounced at intermediate and large scattering angles, especially in polarisation. The SA camera will measure the vertical and horizontal polarisation in the Sun and anti-Sun directions as Huygens spins. These measurements will be performed at two wavelengths (500 nm and 935 nm) to provide sensitivity over a wide range of altitudes and particle size.

The SA camera's angular sampling characteristics are listed in Tables 1 and 3. Measurements at small solar angular distance are made when the Sun is behind the shadow bar, as viewed from the SA camera window. The solar zenith angle during descent is near 50°. In the sunward direction, the camera covers scattering angles of 5-25°. During the measurement in the anti-Sun direction, the scattering angle coverage is 75-125°, on a 1° grid (see Fig. 3). Each measurement samples the total column above the Probe. The aureole contribution from a 2 km layer of the atmosphere is found by taking the difference between two measurements.

When measurements are collected near the Sun, the shadow bar prevents direct sunlight from striking the solar aureole window assembly. A beam splitter is used to provide input from a calibration lamp. Calibrations are performed several times during the cruise to Titan and occasionally during the descent. They are made in such a way that signal from the atmosphere can be subtracted from the total.

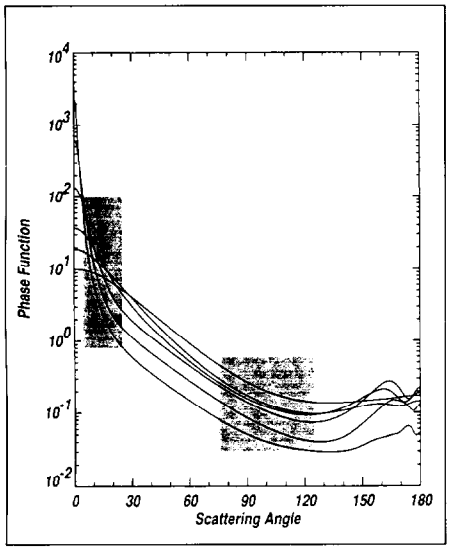

Fig. 3. The Solar Aureole camera samples the scattering angle ranges shown by the shaded regions, for a solar zenith angle of 50°. Also shown are phase function curves for spheres having a log-normal size distribution with mode radii ranging over 0.0625-2 μm doubling each time, at a wavelength of 0.5 μm. The smallest particles have the smallest forward-scattering peak.

A telecentric micro-lens design provides wide angular coverage at f/2 for the solar aureole system. The polarisers used for the visible and near-IR channels are quite pure; the polarisation they impart to unpolarised light will be within a few percent of 100%. The Mueller matrices of all the optical elements will be calibrated before launch, allowing an accurate measurement of the intensity of vertically and horizontally polarised light during descent. Optical fibre ribbons are located at the foci of the camera lenses. They merge with fibre ribbons from the other visible optical elements to feed the focal plane, as shown in Fig. 1.

The use of solar aureole measurements to retrieve particle size distributions is well known, and several retrieval algorithms have been described in the literature (see, e.g. Dave, 1971; Nakajima et al., 1983). Accurate retrievals require a high signal/noise ratio. The SA camera was designed to achieve $S/N \geq 100$.

The $6 \times 50°$ solar aureole FOV maps onto a 6×50-pixel area of the CCD. Calculations show that S/N will be >100 provided that six pixels are summed. Pixel summing will be performed during data analysis by summing pixels along arcs with constant angular distance from the Sun. In this way, no angular resolution will be lost to pixel summing. The expected S/N varies from ~ 100 to ~ 900, depending on wavelength, altitude, solar zenith angle and azimuth during the measurement interval between 160 km altitude and the surface.

3.5.5 Violet photometers

The purpose of the violet photometers is to extend the spectral range of the measurements to 350 nm from the visible spectrometers' short wavelength limit of 480 nm. As no sharp spectral features are expected in this spectrum, a single spectral channel is used. In this spectral region, the spectrum of the incident sunlight is

modified by the absorbing properties of the small photochemical aerosols in Titan's stratosphere. These particles absorb more and more of the short end of the spectrum with increasing depth into the atmosphere. Hence, in order to measure the energy deposition, it is important to filter the response of the detectors to make them relatively spectrally flat so that the violet measurements can be converted to absorbed energy independent of assumptions regarding the spectrum of the light measured. We specify that the product of the spectral response of the violet detectors and the transmission of the violet filters to be spectrally flat to 10% from 350 nm to 480 nm for these measurements.

The Upward-Looking Violet (ULV) photometer shares the ULVS system diffuser; its FOV is identical to that of ULVS. The shadow bar permits separation of the direct and diffuse downward flux in the violet in the same way as for the ULVS, and the sampling in azimuth is the same for the ULV and the ULVS systems. The DLV uses exactly the same baffle and diffuser design mounted on the bottom of the sensor head to measure the upward violet flux, but without the shadow bar. The DLV's sampling in azimuth is limited to two regions, near the Sun's azimuth and near 180° from the Sun. These two measurements sum to give the total upward violet flux.

For the sake of simplicity, the electronics for the ULV/DLV systems use the same 12-bit A/D converter used for several other housekeeping functions, including voltage and temperature monitoring. The light level in the upward-looking violet channel at the top of the atmosphere is known from the solar spectrum. A single gain with a fixed time constant is used in the ULV system with no provision for gain change or change in integration time in flight. The gain is adjusted when the instrument is built so that the sum of the signal from the inflight calibration signal and the downward solar flux at Titan occupy between half and three-quarters of the 4096 available digital steps. The signal from the inflight calibration system is adjusted to be roughly equal to the signal expected from the Sun at descent start. This gives about 1000 digital steps for the violet signal at the start of descent. The random noise in the ULV channel is comparable to the size of a digital step. We can measure the absorption of the violet energy in the ULV's bandpass during descent to a few tenths of a percent of the value at entry.

3.5.6 Sun Sensor

The timing of all of the upward-looking DISR measurements requires precise knowledge of the solar azimuth angle. To satisfy this need, a Sun Sensor is located beside the shadow bar. The sensor's FOV is a 64° cone centred 47° from the zenith. The SS consists of a window, lens system, filter, reticule, a pair of lenses to focus the light on the silicon photodiode detector, and its associated readout electronics. As the Sun crosses the FOV, three large pulses are seen as its image enters the three slits of the focal plane reticule. A detection circuit locates it in the central slit to define zero azimuth angle. The first and third slit are tipped with respect to the centre slit to permit determination of the Sun's zenith angle. The times of all three slit crossings are transmitted in housekeeping. The times between the three crossings compared to the times between successive crossings of the centre slit (the rotation period) give the Sun's zenith angle and the Probe's attitude on each rotation.

In addition, the brightness of the central pulse in each rotation past the Sun is included in the telemetry to give a measure of the direct solar beam at the wavelength of the SS system (939 nm) as a function of altitude. The SS is designed to track the direct solar beam down to 1/1000 of its brightness outside Titan's atmosphere. At the nominal solar zenith angle of 50°, the Sun signal would be lost at a vertical extinction optical depth of 4.4. This compares to a vertical optical depth of less than about 1 in some current Titan models at the Sun Sensor's wavelength.

The SS uses several logic tests on the relative timing of the three-pulse series on successive rotations to distinguish pulses due to the Sun from variations in intensity

that might be due to diffuse clouds above the Probe. If Huygens falls beneath a thick cloud and loses lock, the internal rotation rate transmitted by the Probe's spin sensor is used to time DISR data collection. DISR's Sun Sensor continues to look for the Sun after losing lock, and will find it if it reappears from behind a passing cloud.

3.5.7 Internal calibration system

Almost all of DISR's science goals require measurements to be made on an absolute photometric scale. This is difficult enough for a single optical system and detector, let alone for a system as complex as DISR. In principal, the measurements of the Sun's apparent brightness at high altitude near the start of the descent at some IR wavelengths may be relatively unaffected by atmospheric scattering and absorption, and so may provide an important check on the absolute calibration of this one DISR optical system. The ability to tie all the various DISR systems together on a single photometric scale is provided by the internal calibration system built into the DISR Sensor Head.

The internal calibration system consists of a set of three redundant 1 W lamps that illuminate one end of a bundle of thick quartz fibres. Each fibre carries some light from the calibration lamps to the first optical element in each of the other DISR optical systems. This light is reflected from either the inside of the window for that system or from a small reflector mounted on the back of the window and passes through the rest of that optical system to the detector. The fraction of the light from the calibration lamps carried to the input of each DISR measuring sub-instrument is carefully measured before launch, and expected to remain constant throughout the mission. We should be able to track changes in the sensitivity of detector pixels, in the transmission of the imaging fibre optic conduit or in other optical elements, during cruise by monitoring the relative outputs of each DISR system to the light provided by the internal calibration system.

It is important to emphasise that we are not relying on the stability of the absolute output of the internal calibration system lamps, only on the stability of the relative fraction of the light carried to each DISR subsystem by the thick quartz fibres of the calibration system. These fibres are not expected to be susceptible to darkening from energetic particle bombardment. Thus, the changes in the relative output of the different DISR optical pixels can be tracked with time after launch and even measured several times during Titan entry.

There are no moving parts in the internal calibration system, so the light from this system is added to that from the ambient Titan atmosphere during descent. The light from the calibration system is designed to exceed that from the ambient atmosphere by a large factor. In addition, we have designed the internal calibration procedures to collect light with the calibration lamps on, then off, and then on again at the same azimuth in each case to permit relatively accurate subtraction of the ambient signal from the signal provided by the calibration system. The calibration light levels are adequate to make measurements with S/N better than the target value of 100 for measurements of the ambient atmosphere.

3.5.8 Surface Science Lamp

The purpose of the Surface Science Lamp (SSL) is to illuminate Titan's surface in spectral regions where strong atmospheric absorption bands prevent sunlight from penetrating to the surface. The SSL permits continuous measurements of the surface's spectral reflectivity to be made throughout the entire spectral range. The SSL is a 20 W lamp with a parabolic reflector that illuminates the surface and fills the narrow $3 \times 9°$ FOV of the IR spectrometer with enough light to give a S/N of 50 at 60 m altitude within the strong methane bands even if the surface reflectivity is as low as 0.05.

The lamp system is activated at 400 m altitude (given by the radar altimeter) and

is operated during the last several minutes of descent, when a continuous sampling of the surface reflection spectrum is obtained using both the DLVS and DLIS.

3.6 Mechanical design

The DISR instrument consists of two packages: the Sensor Head and the Electronics Assembly. These are mounted on top of the Probe's instrument shelf. The SH is mounted on a metal bracket above the instrument shelf and sufficiently far outboard so that its front protrudes through the Probe's back side. This permits clear views from the zenith to the nadir and in directions to $\pm 85°$ in azimuth from the radial direction (see Fig. 4).

The EA (see Fig. 5) is a straightforward box containing six boards mounted horizontally above the power supply that is built into the chassis base. The six boards, each 12.7×20.8 cm stacked 1.5 cm apart, include the CCD drive board provided by MPAE, the data compression board provided by TUB, the IR detector system driver board provided by the Paris Oobservatory, and the digital board, CPU board and auxiliary board provided by Lockheed Martin. The EA's 4.4 kg mass includes radiation shielding on particular electronic parts. The EA's box is bolted together from slab sides, top, front and back above the base. The six boards are an integral part of the structure and are bolted to the chassis side walls and the back wall.

The SH's mechanical design, shown in Fig. 6, is a much more challenging task than packaging the EA. The SH assembly must hold the detectors, fibre optics, foreoptics for the visible and IR spectrometers, the three imaging cameras, the Solar Aureole camera, the internal calibration system and the Surface Science Lamp all in precise alignment over a temperature range of some 150°C for 10 years, and throughout the mission's vibration and shock environment. In addition, the detectors' thermal environment must be controlled during descent. The detectors must be protected from the energetic particle environment during the mission. Finally, the size and mass of the package are severely constrained as well.

The SH can be thought of as having a CCD detector side and an IR side. The face of the CCD is held 20 μm from the end of the fibre optic conduit that delivers light from the three imagers, Solar Aureole input assembly and visible spectrometers. This conduit and its face that mates to the CCD are shown in Fig. 7. The CCD half of the SH, including the detector, fibre optic conduit, imager lens assemblies, Solar Aureole assembly and visible spectrometer, is shown in Fig. 8.

The IR half of the Sensor Head begins with the pair of IR array detectors and their pre-amp board. This detector is mounted to the IR spectrometer, shutter and fibre input assembly, as shown in Fig. 9.

The two detector assemblies are surrounded by a tungsten radiation shield 4 mm thick, sufficient to prevent protons of <64 MeV from reaching the detectors, significantly reducing the radiation dose.

The optical systems are securely mounted to a titanium optical bench that is secured to the base of the SH housing using a ball joint and two slip joints. This bench ties all the optical systems to the detectors. Fig. 10 shows how the optical bench assembly fits into the SH box. Figs. 11 and 12 show the optics assemblies after insertion into the main SH box. These views show the Surface Science Lamp, Sun Sensor, the three imager lenses, visible spectrometer and the input optics assemblies for the Solar Aureole system and the visible and IR spectrometers. Several calibration fibres that bring light to the input optics are also visible.

The DISR thermal design must maintain interface constraints, cool and maintain the detectors' temperature within limits, maintain all other components within their temperature limits, and minimise mass and power. In particular, it is important that the detectors are cooled as rapidly as possible from their temperatures near 260K at Titan entry to below some 220K in order to minimise the influence of dark current

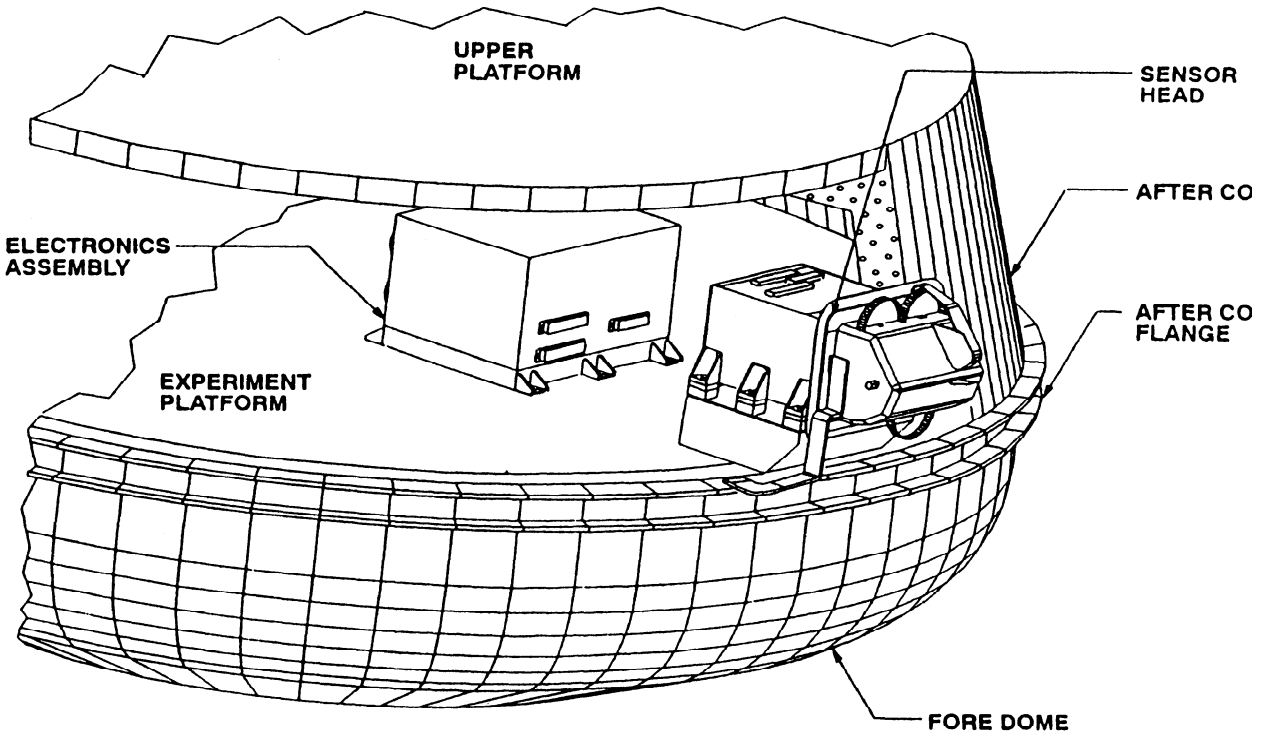

Fig. 4. The arrangement of the Electronics Assembly and the Sensor Head on Huygens' instrument shelf.

Fig. 5. The Electronics Assembly box.

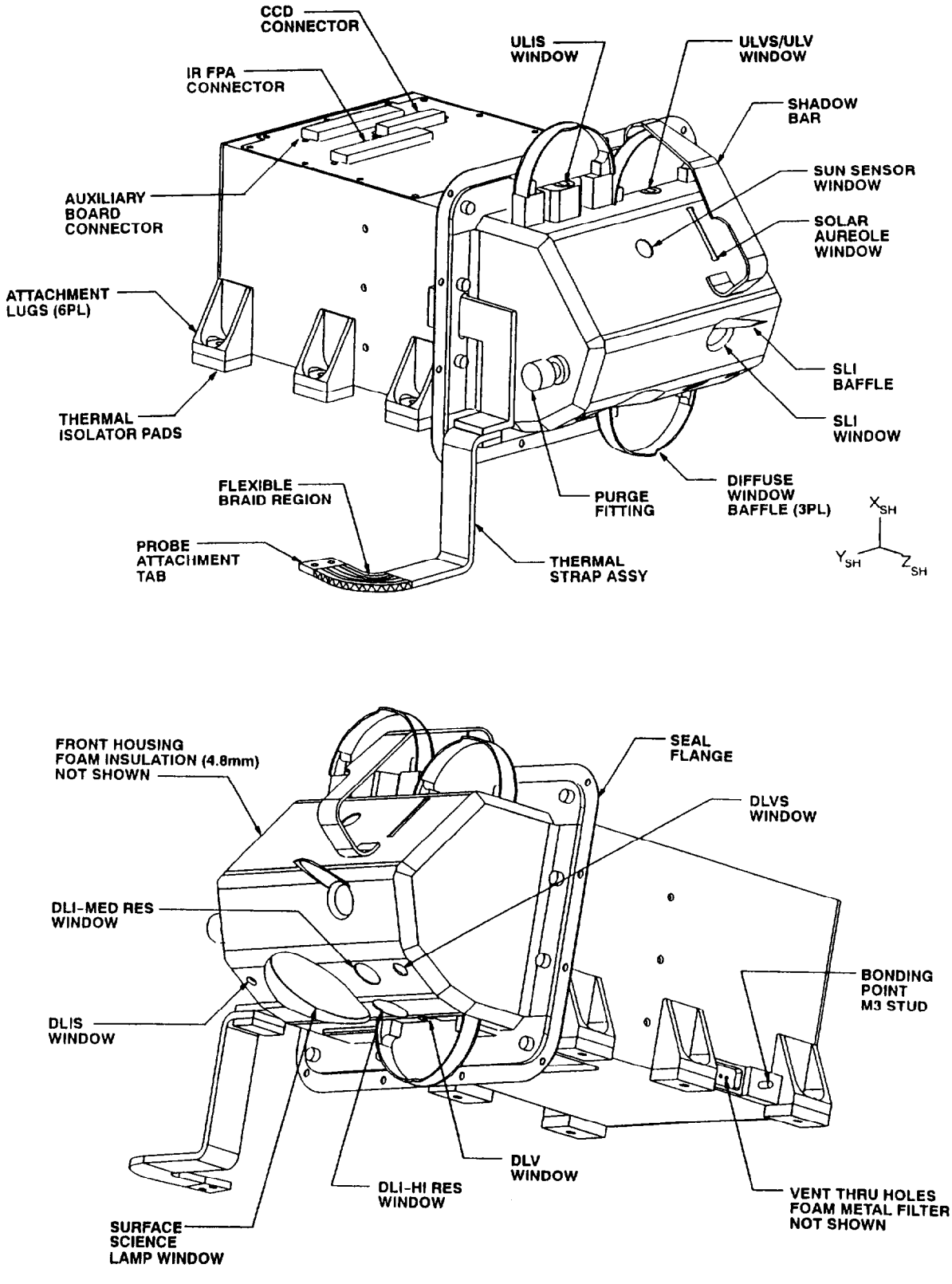

Fig. 6. The Sensor Head as seen from above and below.

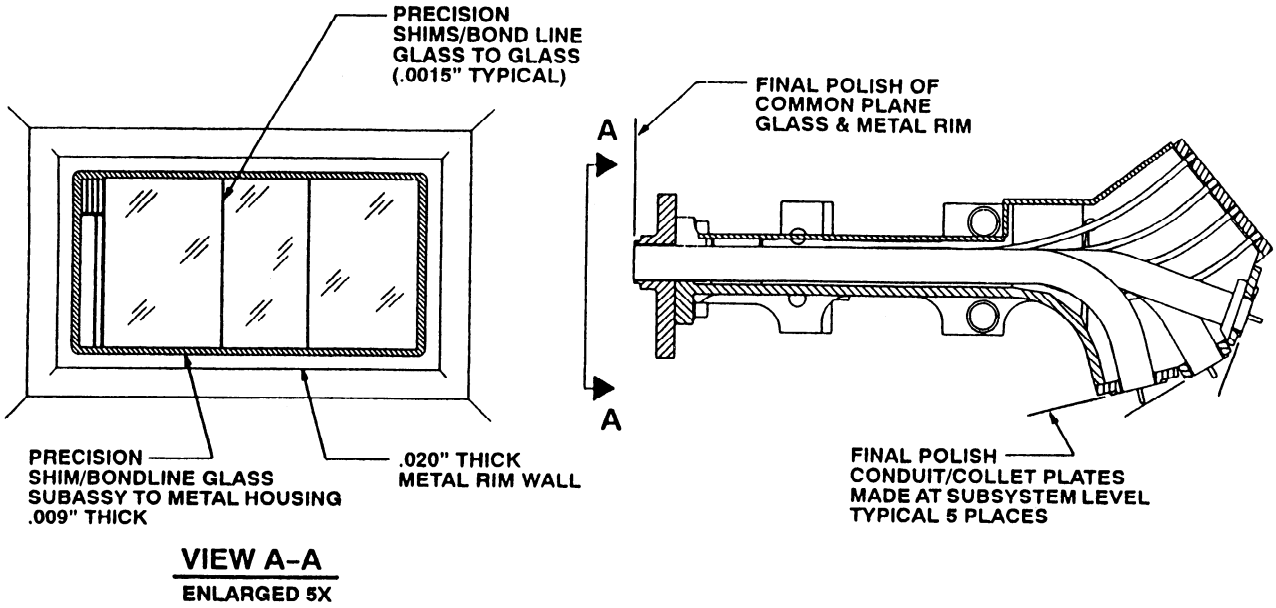

Fig. 7. The fibre optic conduit, including the end view that mates with the CCD detector.

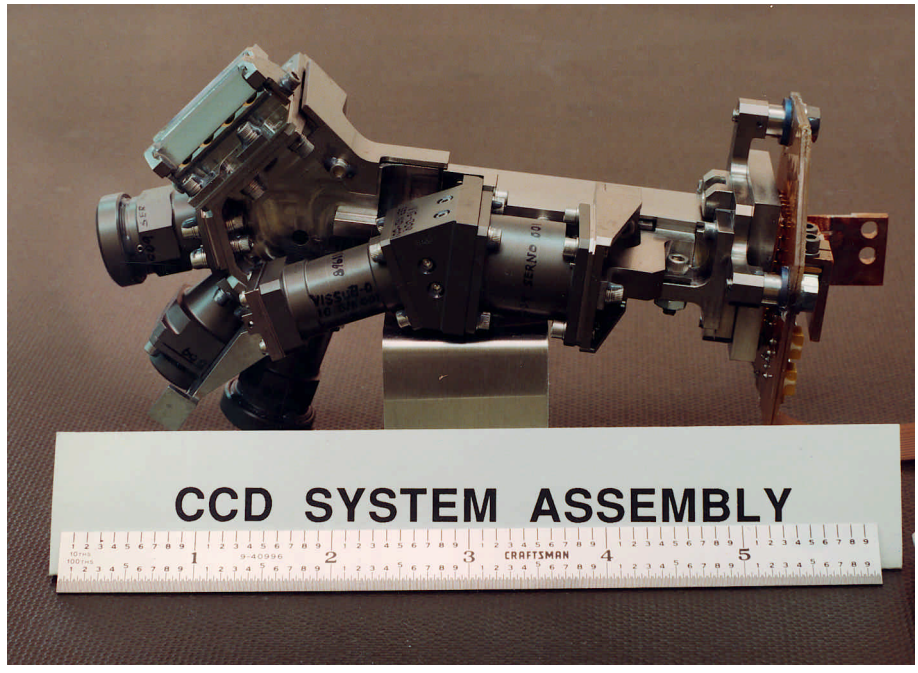

Fig. 8. The CCD mated to the fibre optic conduit, three imager lens assemblies, solar aureole input lens assembly and visible spectrometer.

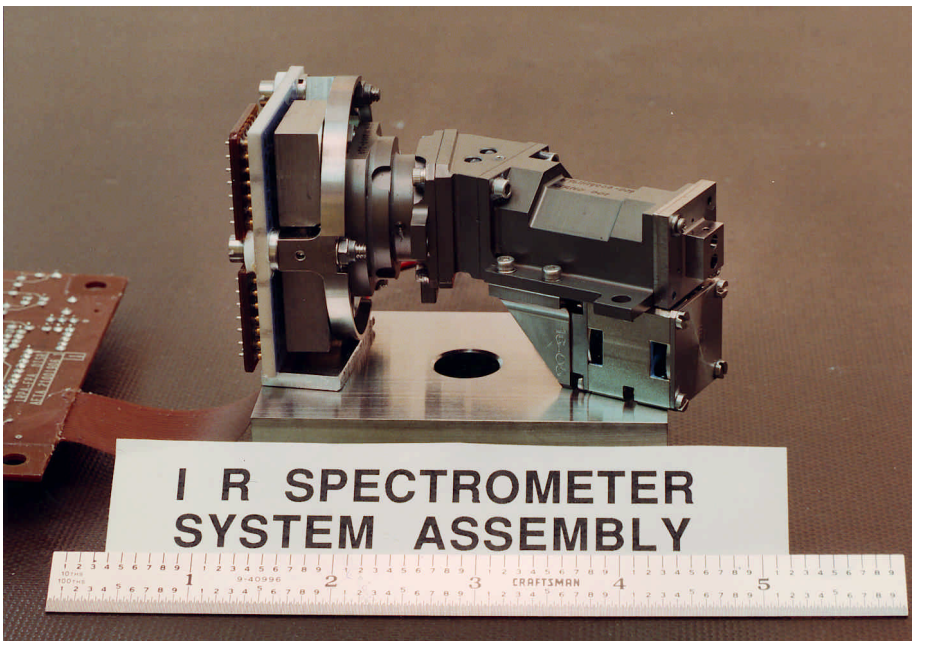

Fig. 9. The IR detector mounted to the IR spectrometer, the shutter and the input fibre collet.

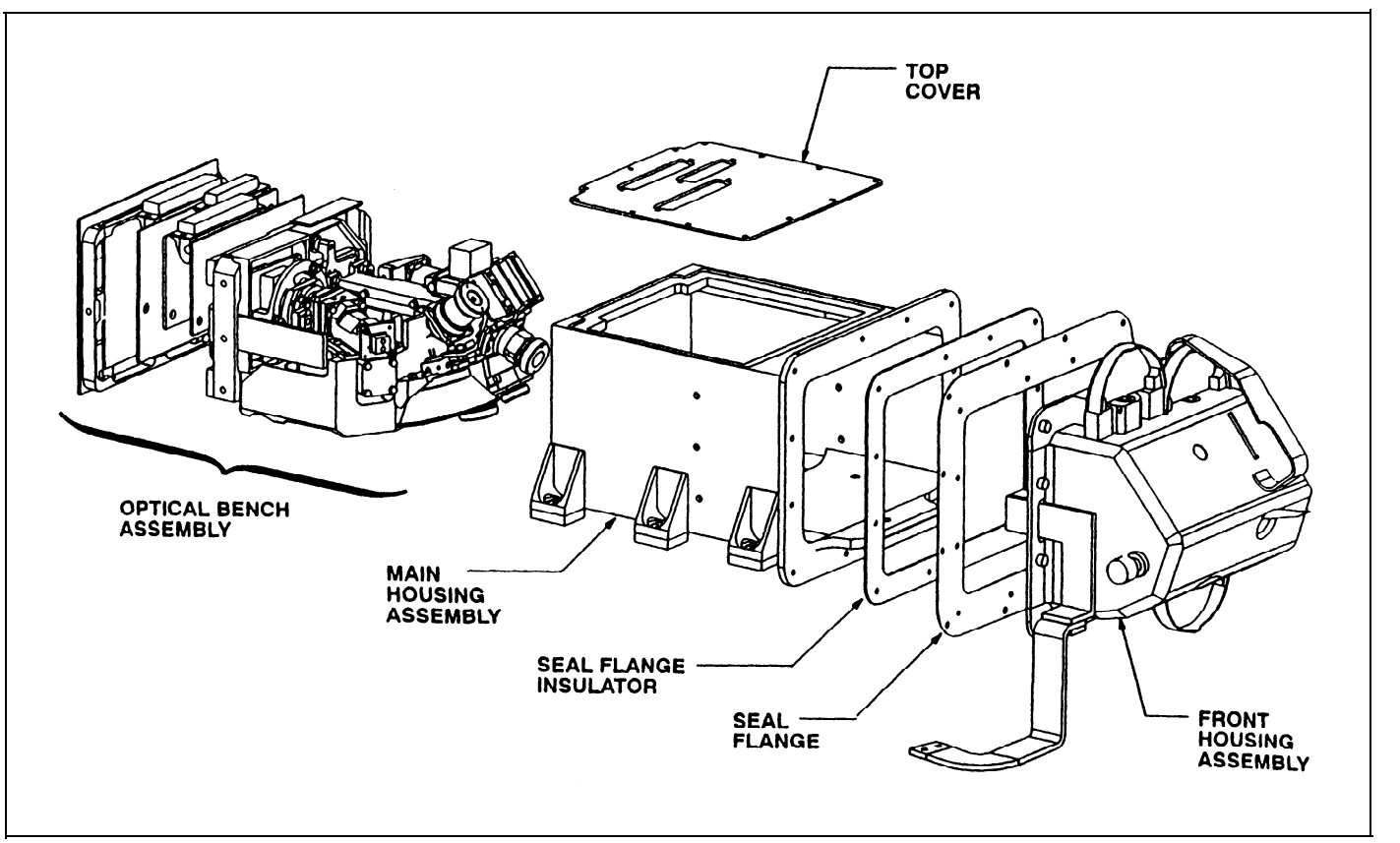

Fig. 10. The optical bench assembly and how it fits into the Sensor Head package.

Fig. Il. The optics after insertion into the main Sensor Head box.

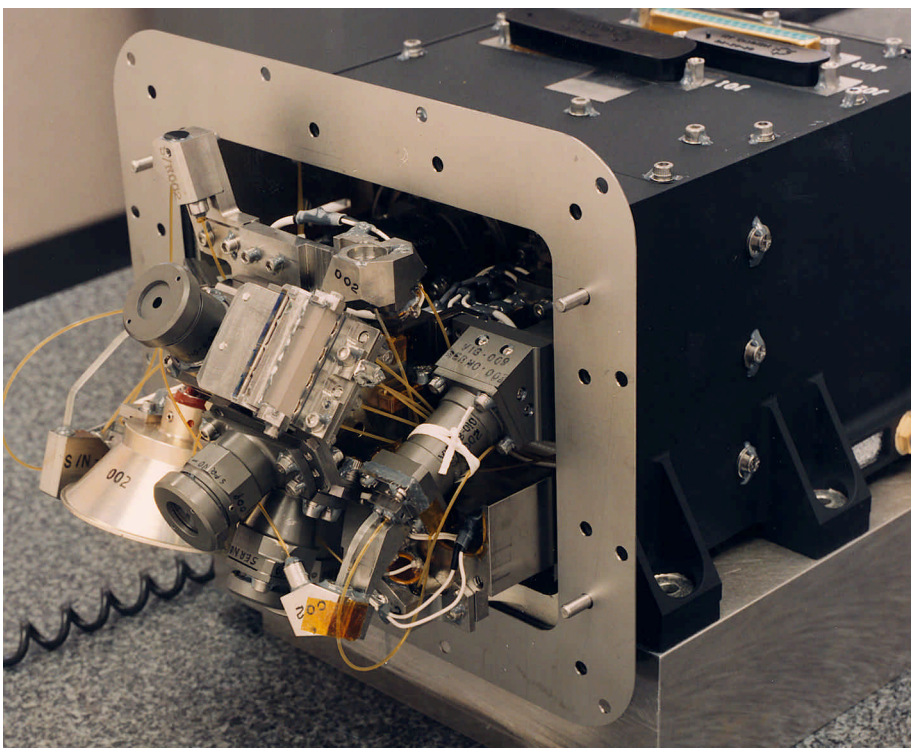

Fig. 12. The Sensor Head before the front housing is installed. The Sun Sensor, Surface Science Lamp, imager lenses and inputs to the DLIS and DLVS are visible, along with some of the calibration fibres bringing light to the input optics.

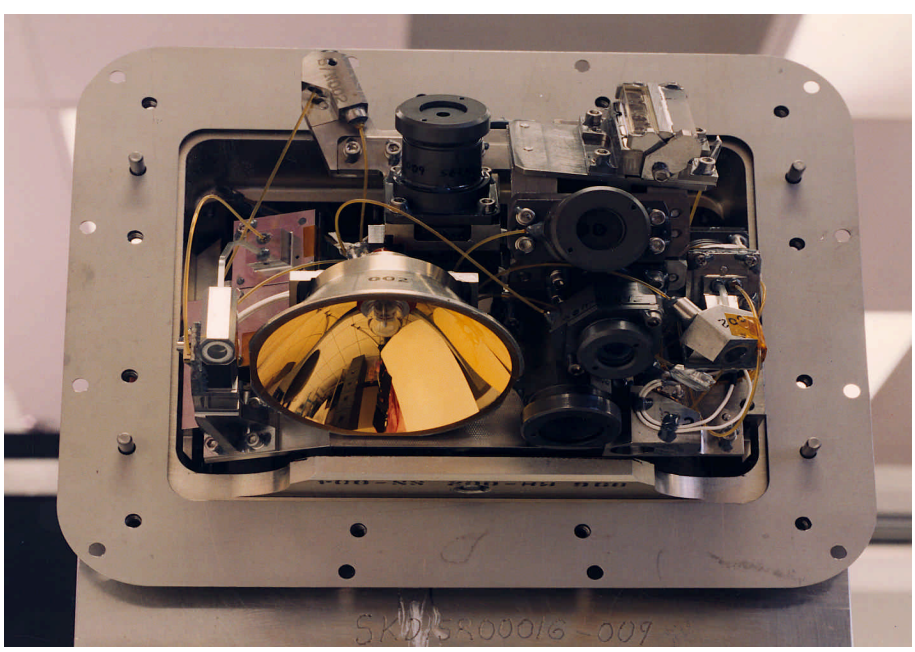

and to ameliorate the defects in CCD pixels that may have been damaged by energetic particle impact during cruise.

The detector cooling system includes a thermal strap to provide a heat sink to the atmosphere via an attachment to the Probe. A heater ensures that the detectors will remain above their minimum temperature limit, thermostatically controlled to maintain >160K. The housing coupling and the detector components masses are minimised to allow a rapid cooldown. The temperatures of the PC boards in the SH are maintained with a second electronic thermostatically-controlled heater.

The SH housing is constructed of aluminum to provide interior-exterior thermal coupling. This will maintain the exposed windows well above the ambient atmospheric temperature. The exposed portion of the housing is covered with a low density insulation and coated with a conductive paint. The interior housing is conductively isolated from the Probe but radiatively and convectively coupled to it. This allows Huygens to provide some heating of the SH 'warm' components. The SH front housing is thermally isolated from the rear housing.

3.7 Compression of imaging data

Imaging data are compressed onboard before transmission in order to achieve a balance between the number and the quality of images received. The imaging data are digitised at 12 bits/pixel. They are first divided by an onboard flat field to eliminate artifacts introduced by variations in the transmission of the fibre optic conduit. They are then reduced from 12 to 8 bits/pixel using a pseudo-square root software algorithm (see below). They are then passed to a lossy hardware data system for further compression.

Simulations with a series of test images have shown that, in principal, lossy compression by the standardised JPEG scheme is applicable. For most of the scenes, the image distortions are relatively small for an additional compression by a factor ≤ 8. Accordingly, the JPEG algorithm has been selected as the baseline. Implementation of such a compression by software running on the main processor would limit the image cycle time to >1 min. Therefore, a dedicated hardware coprocessor has been developed which (1) performs a complete compression of a 256×256-pixel image within <130 ms, (2) dissipates about 120 mWs per compression and <200 mW in idle mode, and (3) is implemented on a single multilayer board of 215 g. The coprocessor is designed around an STV3200 DCT chip, an 80C86 microprocessor and eight ACTEL FPGAs. The compression algorithm running on this dedicated coprocessor deviates in some aspects from the JPEG scheme in order to make the hardware less expensive in terms of power and mass, and to enhance the robustness against transmission errors.

Fig. 13 shows the data flow through the coprocessor. The first very basic operation is transformation of the image data from the spatial domain into the frequency domain. The applied Discrete Cosine Transform (DCT) concentrates most of the image energy in a small set of highly decorrelated, low frequency coefficients. The primary compression mechanism is to represent the minority of lumped high energy coefficients with higher accuracy than the majority of low energy coefficients. Even deletion of most of the low energy coefficients removes only a small portion of image information. Accordingly, the coefficients below a given threshold are deleted and the remaining coefficients are requantised with an adjustable step width proportional to a value Q. Subsequent zigzag-ordering concatenates coefficients of similar spatial frequency and generates a coefficient string where typically a bulk of low frequency/high energy coefficients is followed by some spurious high frequency coefficients, which are separated by long intervals of zeros acting as placeholders for the deleted coefficients. Run length encoding exploits this specific string structure.

In the next step, the original JPEG scheme applies Huffman encoding. This has been

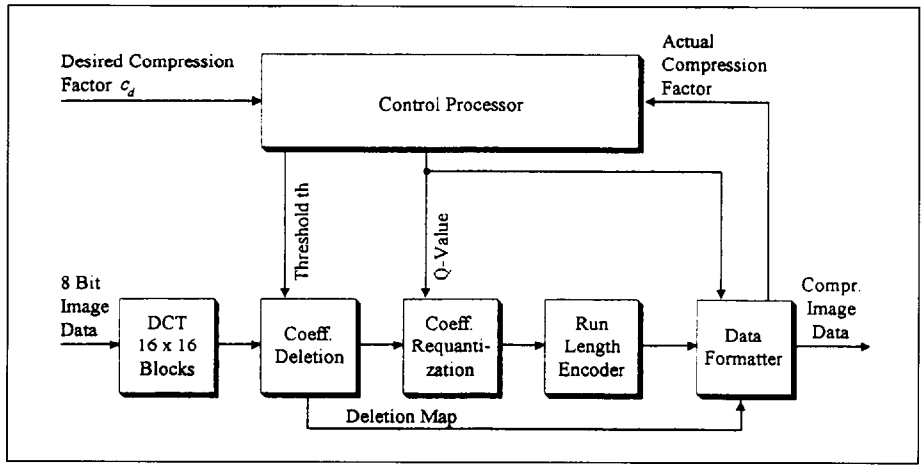

Fig. 13. Data/control flow of the DISR compression algorithm.

replaced by a specific scheme less sensitive to transmission errors at the expense of a slightly reduced coding efficiency. The processing of the frequency coefficients is iterated several times in order to approach a target compression factor of near-optimum image quality, which is expressed by the S/N of the total image. The first run determines the quantisation step width, which remains unchanged for all following runs while the deletion threshold is varied.

The S/N (in the image intensities) of the modified hardware implementation is ≤ 1 dB below the values achievable with standard JPEG. In flat image regions, blocking effects become visible at lower compression factors compared to JPEG. These very limited deficiencies in image quality are regarded to be outweighed by the associated savings in power and mass. On the LENA test image (a standard image commonly used for testing image compression systems), the S/N varies between about 50 and 30 at compression ratios of 3:1 and 6:1, respectively. On simulated low contrast images as expected for Titan, the noise is increased above shot noise by factors of only some 1.7 and 2.5 for compression ratios of 3:1 and 6:1, respectively.

3.8 Electronics

The electrical block diagram of the entire DISR instrument is shown in Fig. 14. The left-hand portion shows electronics in the SH, while the right-hand section indicates the electronics housed in the EA package. The SH contains three small boards: one provided by MPAE contains the CCD's pre-amps; one provided by PO contains the IR detector's pre-amp; and the third, from MMC, provides pre-amps for the Sun Sensor and its test light emitting diode, as well as for the violet detectors of the ULV and DLV instruments. The European Co-Is also provided the EA's three shaded boards: the CCD's driver (MPAE); the IR detector driver (PO); and the hardware Data Compression System (TUB).

The CPU board provides radiation-hard critical RAM in 128 kbytes of program RAM and an additional 64 kbytes of data RAM. It also holds 128 kbytes of PROM and a separate block of 64 kbytes of EEPROM, which can be changed by commanded uploads. The microprocessor is a MA31750 running at a clock speed of 12 MHz capable of some 1.6 million instructions/s (MIPS). Some 1.2 MIPS are required for operation of the DISR as planned. A watchdog timer is provided with a 100 Hz clock at 16-bit resolution.

The Digital Board contains a large (1.5 Mbyte) frame buffer of static RAM accessible by the CPU or by any of three Data Management Assembly (DMA) channels. The entire frame buffer is refreshed every 10 s by CPU block read/write routine using a full Error Detection And Correction (EDAC) function provided by a single Harris Semiconductor chip.

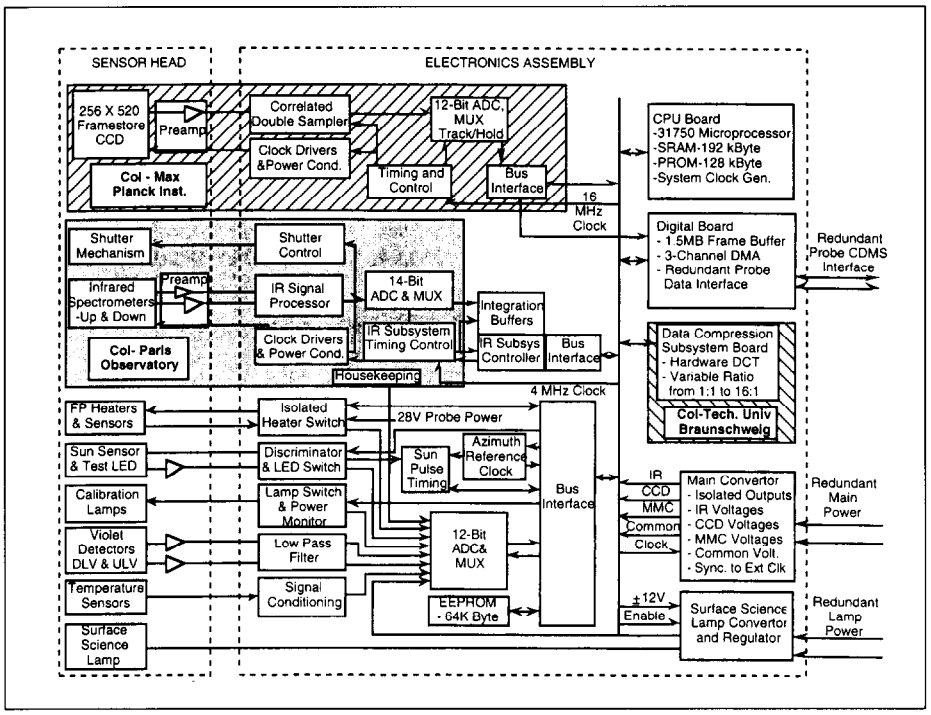

Fig. 14. Block diagram of the electronics on the six boards in the Electronics Assembly. The three cards provided by the European Co-Investigators are shown shaded, and the functions contained on the CPU Board, the Digital Board and the Auxiliary Board provided by Lockheed Martin are shown.

Three programmable DMA channels are provided using Actel 1020 Field Programmable Gate Arrays (FPGAs). The mode, word count, source and destination addresses are all programmable.

The Probe interface provides dual telemetry packet channels for transmitting the science data. It provides dual Memory Load Command channels to receive the data and/or commands from Huygens. Dual serial status channels are also provided to transmit a 16-bit housekeeping status word to the Probe upon request. Redundant channels are also provided to receive the Probe Data Broadcast data such as spin rate, time and altitude. This interface also provides a means of receiving an indication of which telemetry channel is to be used for commanding the DISR.

The Auxiliary Board contains the digital interface to the IR detector system. It also contains several analogue circuits to: condition signals from the ULV, DLV, Sun Sensor and the Inflight Calibration System; control the focal plane and SH electronics card heaters; monitor temperatures, lamp currents and other housekeeping data in the instrument. A multiplexer and a 12-bit A/D converter are used on the Auxiliary Board for this purpose.

3.9 Software and data collection modes

The DISR flight software was developed using an object-oriented design in the ADA language. The software uses a re-entrant event dispatcher to control execution based on the priorities of events occurring in both the hardware and software. Multi-tasking is not used. Hardware interrupts are used to provide services for the Probe interface, Sun Sensor, general purpose event timer, telemetry channels, direct memory access controllers, CCD, IR detector and hardware data compressor. The software controls the calibration and surface science lamps. The calibration lamps are turned on during appropriate parts of calibration cycles. All commands to the DISR are processed by the software. Only six commands exist, although some have a variety of parameters.

1. A receipt-enable telecommand must begin a commanding session. This command is used to protect against spurious commands
2. A change-mode telecommand may be used to change the DISR's operating

mode into descent mode (the default mode), calibration mode, single telecommand mode or memory access mode
3. Single measurement telecommands direct the instrument to perform one or more repetitions of a particular measurement. These commands are useful during instrument calibration and test
4. Single test telecommands are similar to single measurement telecommands, except they initiate preprogrammed test sequences on the specific portions of the hardware, including the IR shutter, hardware data compressor, heaters and lamps
5. Memory upload commands are used in memory access mode to store new tables that are read by the software. These table entries include bad pixel maps, square root compression tables, and parameters that control measurement scheduling and processing
6. Memory dump telecommands can transfer any portion of DISR memory into telemetry for verification.

The software also coordinates and controls all data collection. Optimum exposure times are computed for each sub-instrument using the CCD and IR detectors. These times are based on the data number population histograms of the most recent previous exposure of the same type. The exposure time can also be limited by the amount of smear caused by the Probe's spin.

Onboard data processing functions also include several miscellaneous functions. Adjacent pixel columns may be averaged within the same instrument FOV. Data for the hardware data compressor must be reformatted before it is fed to the compressor. Lossless compression is done entirely in software. Bad pixels are eliminated according to a bad pixel map stored in EEPROM. Data from the imagers are also reduced from 12 bits to 8 bits before being fed to the hardware data compressor. This reduction is done using a table lookup that performs a pseudo-square root transformation of the raw data. A watchdog timer can reset the microprocessor if it times out. The software that builds telemetry packets periodically resets the watchdog timer. If telemetry is not being produced, the processor will be reset and execution will be restarted.

Calibration and instrument health data are collected at 6-month intervals during cruise. One of five possible activities may be performed at each opportunity. The Health Check sequence exercises each software-controlled function to test for normal operation. The In-Flight Calibration sequence is used to obtain relative response and measure the noise level of the detectors. The Simulated Descent tests descent sequencing using the parameters loaded into special tables. Two types of activities are available for contingencies. Single Measurement and Single Test commands can be used to diagnose problems with specific instrument subsystems. Finally, memory dumps and uploads can be used to verify the contents or memory and to upload new table values to correct for instrument subsystem malfunctions.

One of the software's more interesting aspects is the way it optimally schedules collection of related data from various sub-instruments. During descent, data collection is divided into cycles that form a coordinated set of measurements within a limited time span. Several different types of cycles are used to meet the differing needs of data collection during different parts of the descent. The software uses information from Huygens, including the altitude, time and spin rate, to decide which type of cycle to start next. The choice also depends on the amount of buffer space available within DISR and on the current Probe telemetry rate. The software chooses a cycle type that will gather sufficient data to keep the instrument from running out of telemetry packets, yet it must also choose one that will not provide so much data that it overfills the available buffer space.

Differing requirements are placed on the data buffering scheme depending on how

close Huygens is to the surface. Normally, data can be gathered much faster than they can be telemetered. If the Probe is still high enough to allow sufficient time for telemetry before impact, data may be profitably buffered, allowing the buffer to fill further as each cycle passes. On the other hand, if Huygens is near the surface, each data set should be telemetered as soon as it is complete in order to prevent the Probe from hitting the surface with substantial amounts of data still in the buffer.

Early in the descent, Huygens is falling rapidly. It is important to measure quantities such as the solar flux deposition and the solar aureole profile within vertical intervals that are small compared to the atmospheric scale height. Cycles high in the atmosphere are driven by a cycle duration constraint, even if many cycles spend a long time in the buffer before they are telemetered. However, at some altitude it is important to start each new cycle with almost nothing in the buffer. The most recent, lowest altitude data will be transmitted immediately if the buffer is in this state.

We use both of these scheduling algorithms during the descent. Above 20 km altitude, we use duration-constrained scheduling. At 20 km, we pause to permit all previously buffered data to be telemetered. After this, new cycles are not begun until only a few telemetry packets remain in the buffer.

Within data cycles, it is usually important to schedule measurements at particular azimuths. Images, for example, must be scheduled to occur at 12 equally-spaced azimuths to provide data for a mosaic. The software determines the azimuth at the beginning of each cycle and predicts its change with time during the cycle using a quadratic extrapolation. As new information about the spin rate comes in from the Sun Sensor, these predictions are updated during the cycle and measurements are scheduled using them.

4. Measured Quantities

The altitudes and times during descent where various types of cycles are gathered are shown in Fig. 15. The instrument is turned on near 170 km altitude. In order to fill the initially empty telemetry buffer as rapidly as possible, the instrument begins with a data collection cycle that contains an image panorama. The data collected in cycles containing image panoramas are shown in Table 3. Note that on alternate cycles of this type, the images' azimuths are offset by 15°, half the width of the images. These cycles contain a full set of spectral data (with downward-looking visible spectra in the centre of each image) and solar aureole data as well. Above 20 km, these cycles are constrained to collect all their data in 1.5-4.5 min.

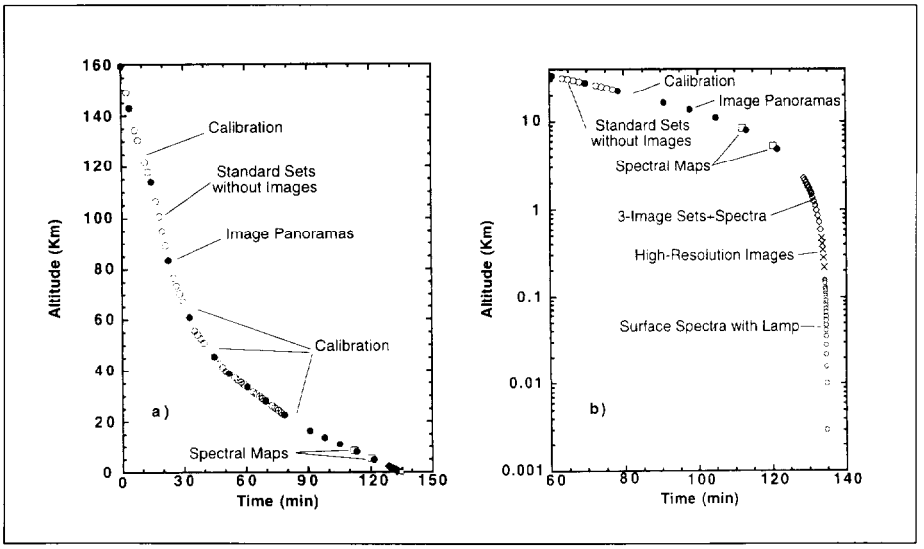

Fig. 15. Vertical profile of various types of data sets obtained during Titan entry. The variation throughout the entry is shown in (a), and the variation at low altitude is emphasised in (b).

Table 3. Image cycle measurements.

Sub-instrument	*Azimuths (degrees)*
Solar Aurcolc	1.5 (under the shadow bar), 174
ULVS and ULV	5.5 (under the shadow bar), 140, 180, 320, 338
HRI, MRI, SLI, DLVS	2, 32, 62, 92, 122, 152, 182, 212, 242, 272, 302, 332 or 17, 47, 77, 107, 137, 167, 197, 227, 257, 287, 317, 347
Dark current	180
ULIS	315-45, 290-315 and 45-70, 90-135 and 225-270, 135-225
DLIS	0-45, 45-70, 90-135, 135-180, 180-225, 225-270, 290-315, 315-360
DLV	0, 180

Above 20 km altitude, a non-imaging cycle is chosen as the next cycle if the DISR telemetry buffer contains data that will take more than four additional minutes to transmit. Non-imaging cycles are interleaved between imaging cycles to produce spectral measurements at higher vertical resolution than would be possible if all cycles contained image panoramas. The time for data collection in non-imaging cycles is limited to 1.5-3 min. The maximum cycle duration prevents long gaps between observations that might occur at very slow Probe rotation rates where a cycle might take a very long time to complete. The minimum cycle time forces the scheduler to wait before the beginning of the next cycle and is used to tune the relative numbers of imaging and non-imaging cycles. Increasing the minimum cycle duration allows the telemetry buffer to be emptied further during the cycle, and increases the likelihood that an imaging cycle will be chosen next.

The standard non-imaging cycle differs from the imaging cycle in three respects:

1. six (rather than 12) DLVS spectra are obtained evenly distributed in azimuth beginning 20° from the Sun
2. no HRI or MRI images are obtained
3. six SLI images are obtained evenly distributed in azimuth beginning 15° from the Sun's azimuth.

The SLI data in the central 26 columns of each image are summed to a single column of brightness as a function of zenith angle, losslessly compressed and included in the telemetry stream.

Special calibration cycles are performed four times above 20 km at roughly equally-spaced detector temperatures. These data use the onboard calibration lamps to provide signals dominating those of Titan's. These cycles provide relative calibrations of the upward- and downward-looking sub-instruments as well as corroboration of the flat field properties of the CCD and IR detectors. A special long exposure measurement is also made with the IR sub-instrument while the shutter is closed for accurate determination of the dark current generation rate for each pixel.

At 20 km altitude a special 'pause' cycle occurs in order to empty the telemetry buffer. Imaging cycles are then gathered between 20 km and 3 km, with each new cycle beginning only when the telemetry buffer drains to a preset low level. This sequence is interrupted twice (near 9 km and 4 km altitude) for the Spectrophotometric Cycles when downward-looking spectra are obtained as rapidly as possible for one Probe rotation. These data map the surface's spectral reflectance at high spatial resolution.

If normal image cycles were continued below 3 km, telemetry of the data would not be completed before surface impact. Therefore, between about 3 km and 500 m, special cycles are used in which a set of HRI, MRI, SLI images, spectra and solar

aureole measurements are obtained as rapidly as the telemetry rate permits, regardless of the azimuth (see Fig. 15b).

Between 500 m and 200 m, single HRI images are obtained as rapidly as the telemetry rate permits (about every 8 s). Single HRI images and dark current measurements are the only data collected in this altitude interval. In the last image, near 200 m, the scale will be about 20 cm/pixel.

The Surface Science Lamp is turned on at 400 m altitude. For the final 200 m, we obtain only DLV, DLVS and DLIS measurements. Some 19 spectra are obtained with the SSL turned on. These yield continuous surface reflection spectra over the DLIS spectral range for constraining the surface composition. As Huygens continues to rotate slowly while these exposures are collected, each will view a different surface region. Some of the 20 pixels along the DLVS slit will be illuminated by the SSL, and these are telemetered to the ground, permitting the DLIS spectra to be extended to shorter wavelengths. The S/N of these spectra increase as $1/(\text{altitude})^2$, reaching more than several hundred for ground reflectivities exceeding several percent.

If the instrument survives impact, it will collect data according to a special sequence. One purpose of these cycles is to measure transient phenomena such as reflection from any cloud of dust or spray that may result from Probe impact. A set of 10 upward- and downward-looking spectra are collected first using the ULV, ULVS, ULIS, DLV, DLVS and DLIS sub-instruments. Following these spectral measurements, images are taken with the three cameras. The SLI should give images from the foreground to 6° above the horizon. If Huygens survives long enough, it may be possible to see cloud features blown by the wind. Spectra and image measurements sets are then gathered alternately for the remainder of the mission. Approximately 2 min after impact, the SSL is switched off. After that, it is alternately switched on and off every 2 min. All measurements after impact are taken as rapidly as possible until the buffer fills. Then, new measurements are gathered as buffer space allows. A summary of the data collected in various parts of the descent is given in Table 4.

Table 4. Summary of descent data.

Altitude Range (km)	*36-Image Cycles*	*Non-Image Cycles*	*3-Image Sets + Spectra*	*High-Res Images Only*	*Spectra Using Lamp*	*3-Image Sets*	*Spectral Sets*
160-20	10	33	—	—	—	—	—
20-3	5	—	—	—	—	—	—
3-0.4	—	—	20	—	—	—	—
0.40-0.20	—	—	—	2	—	—	—
0.20-0.0	—	—	—	—	18	—	—
After Impact (first 10 min)	—	—	—	—	—	83	93

Total number of images: >600. Total direct, diffuse, upward, downward sets of flux measurements: 68. Solar aureole measurements: 48 in each of two colours and two polarisation states. Surface spectra: 642 in IR, >3100 in visible

5. Expected Results

The ability of the DISR measurements to support the science goals outlined at the beginning of this paper is summarised here. For studies of the thermal balance, the downward total flux is obtained by summing the measurements at two azimuths 180° apart. The corresponding upward flux in the violet is obtained by a similar sum of the DLV measurements. In the visible and near-IR, the azimuth integral for the upward flux is done by averaging the measurements at all azimuths in the DLVS and DLIS. For the DLVS, the data include measurements at a range of nadir angles along the slit.

These data are weighted with the cosine of the nadir angle and integrated in nadir to give the upward flux. For the DLIS, a model is required to connect the DLIS measurement to give the upward flux in the near-IR. The upward flux is subtracted from the downward flux at each wavelength to give the net flux at each altitude. The difference in the net flux between two altitudes gives the energy absorbed by the intervening atmospheric layer. The integral of this quantity over wavelength, divided by the layer's mass and the specific heat capacity of the layer's gas, gives the solar heating rate for this layer.

The radiative cooling rate is computed from the IR opacity, computed from the atmospheric gases and the particles. The particles' IR opacity is computed from their optical properties and distribution determined by other DISR measurements.

The net dynamical forcing can be used in dynamical models to evaluate the wind field, and then compared to the Probe's drift rate as determined from the apparent motions of features in surface images. Fig. 16 shows the coverage of HRI and MRI panoramas over the surface in response to a nominal wind model (Lunine et al., 1991).

Determination of the properties and distribution of aerosol and cloud particles is somewhat complex. The direct downward flux at each wavelength from ULV, ULVS and ULIS is obtained by subtracting the diffuse flux from the total diffuse plus direct flux. The natural log of the ratio of downward fluxes at two altitudes, divided by the cosine of the local solar zenith angle, gives the vertical extinction optical depth of the particles between the two levels at that wavelength. The variation of this quantity with wavelength gives a measure of the volume-weighted size of the particles.

The solar aureole measurements near the Sun give the size of the forward-scattering peak of the single-scattering phase function of the particles above that altitude. At high altitudes, the optical depth in the 500 nm channel is used to determine the width of the forward scattering peak. This peak is caused by diffraction, and its size depends on the mean projected area of the particles. At lower altitudes, where multiple scattering in the blue above Huygens is large, the data in the 935 nm solar aureole channel is used. At intermediate altitudes, the ratio of the diffraction peak in the two wavelengths gives a check on the area-weighted size of the aerosols above Huygens. The solar aureole measurements 180° from the Sun give the shape of the single-scattering phase function and its polarising properties at large scattering angles. The single-scattering polarisation provides a third measure of particle size.

The particle shape is constrained by the projected-area weighted radius, the volume-weighted radius and the polarisation radius. Models of aggregate particles with different-sized monomers and different number of monomers per particle are compared with the particles' size constraints. Comparison of calculations for the determined shape with the measurements give the particle scattering and extinction cross sections at each wavelength. Comparison with the variation of extinction with altitude gives the number density as a function of altitude. Comparison with the

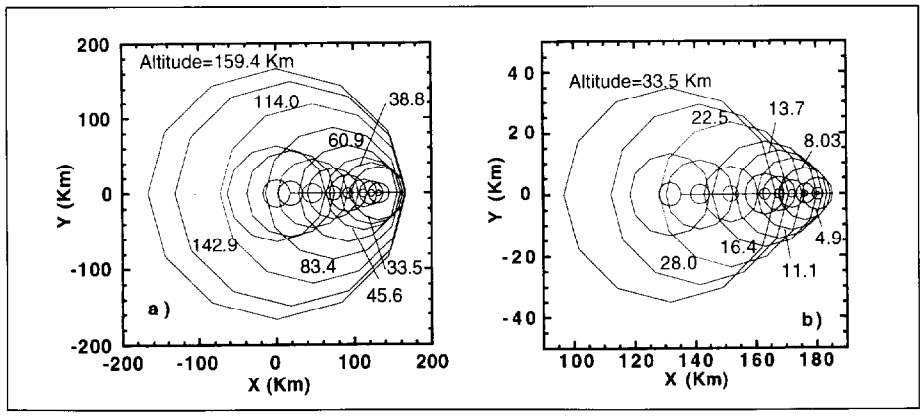

Fig. 16. Coverage of image panoramas on Titan's surface including nominal drift due to wind. (a) image panoramas at altitudes above 30 km altitude. (b) image panoramas below 35 km.

sedimentation rate calculated for these particles gives the particle mass production rate in steady state.

The single-scattering albedo of the aerosols is determined by the change in the net flux at wavelengths where atmospheric gases (primarily methane) do not absorb. The variation of single-scattering albedo with wavelength and the extinction optical depth constrains the imaginary refractive index of the particles as a function of wavelength.

The surface topography is determined both from stereographic analysis of images obtained at different altitudes and by surface photometry and the Sun's known zenith angle. Liquid surfaces can be distinguished by their lack of vertical relief, uniform reflectivities, specular reflections and comparison of their reflection spectra with those of expected mixtures of methane and ethane using the spectra obtained with SSL illumination in the last stage of descent. These reflection spectra can constrain surface composition even if the surface is not liquid. The topography and details of the features seen in the images can reveal the physical properties responsible for forming the surface. The areal coverage as a function of spatial resolution in the images is shown in Fig. 17.

Finally, the profile of methane's mixing ratio is determined from the growth of the many methane features of various strengths observed throughout the descent. The argon mixing ratio is constrained by the methane/nitrogen mixing ratio and the total molecular weight determined by radio occultation data from the Orbiter and the temperature measurements made by Huygens. The DISR spectra will be examined for the presence of other minor constituents as well.

In summary, the DISR suite of measurements has been highly tuned to provide many complementary types of optical measurements designed to contribute to our understanding of the thermal balance, nature of the cloud and aerosol particles, composition and physical state of the surface, and composition of the atmosphere.

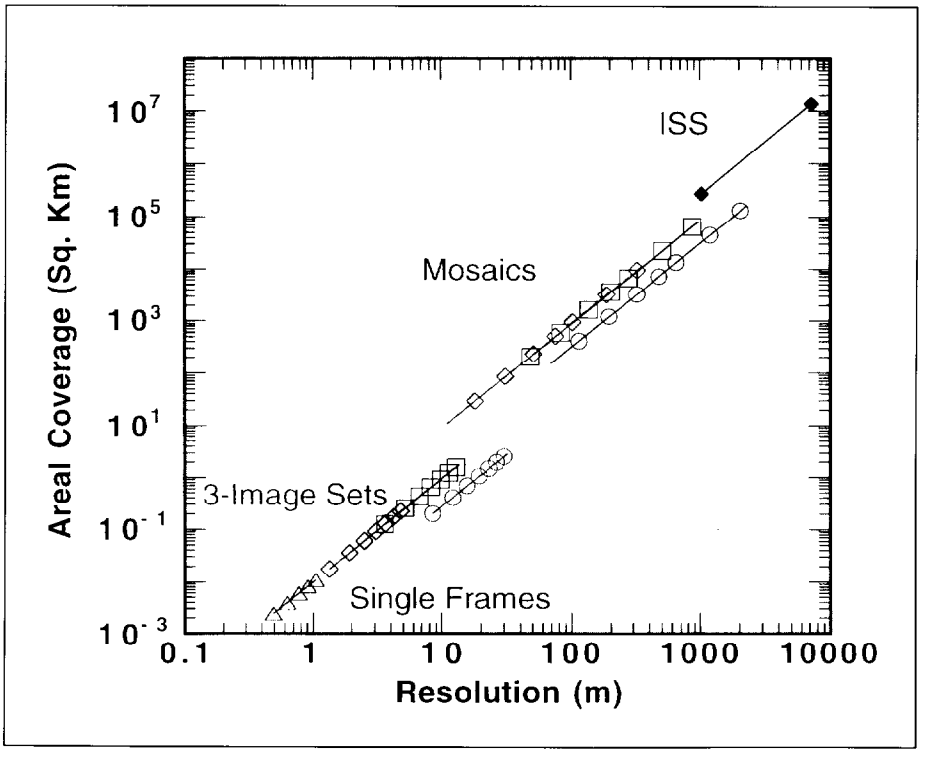

Fig. 17. Areal coverage on Titan's surface *vs* spatial resolution. The coverage and resolution of mosaics made using the SLI (circles), MRI (squares) and HRI (diamonds). Every other panoramic mosiac is shown as a point. Every other frame of the 3-image sets is shown, using the same symbols. The coverage and resolution of each of the five single HRI frames at the lowest altitudes is shown by a triangle. For comparison, the coverage and resolution of the Imaging Science Subsystem camera on the Cassini Orbiter is shown by solid diamonds when Titan fills the frame, and when the frame covers 1/10th of Titan's diameter.

Acknowledgements

The planning, design, development, fabrication and test of the DISR instrument would not have been possible without the collaboration of a large number of dedicated and highly talented individuals. We wish to thank especially the many dedicated contributors at the Lockheed Martin Corporation, Denver for their work on the design and development of the mechanical, optical, electrical and software of the DISR instrument; the engineers and technicians of the Paris Observatory for their work on the IR detectors, support electronics and the shutter; the people of the Max Planck Institut für Aeronomie for their work on the design of the CCD detector and its read electronics; and the engineers of the Technische Universität Braunschweig for their design and development of the data compression hardware. Without the dedicated efforts of all these people, the DISR would not have been possible.

References

Bodin, P. & Reulet, J. F. (1987). A New Channel for SPOT in the SWIR Band. *S.P.I.E.* **865**, 142-149.

Dave, J. V. (1971). Determination of size distribution of spherical polydispersions using scattered radiation data. *Appl. Opt.* **10**, 2035-2044.

Hunten, D., Tomasko, M. G., Flasar, F. M., Samuelson, R. E., Strobel, D. F. & Stevenson, D. J. (1984). Titan. In *Saturn* (Eds. T. Gehrels & M. S. Matthews), University of Arizona Press, pp671-759.

Lemmon, M. T., Karkoschka, E. & Tomasko, M. (1995). Titan's rotational light curve. *Icarus* **113**, 27-38.

Lunine, J. I. (1993). Does Titan have an ocean? A review of current understanding of Titan's surface. *Rev. Geophysics* **31**, 133-149.

Lunine, J., Flasar, F. M. & Allison, M. D. (1991). Huygens Probe Wind Drift: Science Issues and Recommendations, A Report to the Huygens Project.

Muhleman, D. O., Grossman, A. W., Butler, B. J. & Slade, M. A. (1990). Radar reflectivity of Titan, *Science* **248**, 975.

Nakajima, T., Masayuki, T. & Yamauchi, T. (1983). Retrieval of the optical properties of aerosols from aureole and extinction data. *Appl. Opt.* **22**, 2951-2959.

Smith, P. H., Lemmon, M. T., Lorenz, R. D., Sromovsky, L. A., Caldwell, J. J. & Allison, M. D. (1996). Titan's surface reaveled by HST imaging. *Icarus* **119**, 226-349.

West, R. A. & Smith, P. H. (1991). Evidence for aggregate particles in the atmospheres of Titan and Jupiter. *Icarus* **90**, 330-333.